

Fundamentals of High Temperature Processes

The effect of operating parameters and dimensions of the RH system on melt circulation using numerical calculations

Y.-G.PARK *et al.*

Melt circulation as a function of the operating conditions and dimensions of the RH system were calculated using a 3-dimensional numerical model. This numerical model was developed with considering the driving force by gas blowing for melt circulation and was verified from both water model experiments and real RH process results.

Using the numerical model, the influences of various parameters on melt circulation were investigated. The parameters can be divided into two categories, the operating conditions and dimensions of RH system. The effects of each operating parameters such as gas flow rate, the pressure of the vacuum vessel and submerged depth of the snorkel on the melt circulation rate were studied. In addition, the effects of the dimension parameters of the RH system such as the number of nozzles and snorkel diameter were also investigated.

By synthesizing the calculated melt circulation for various conditions, a simple model, which can predict the melt circulation without calculating the three dimensional fluid flow, was developed. Using this prediction model, the effects of the various parameters on melt circulation could be calculated easily.

(*cf. ISIJ Int.*, **41** (2001), 403)

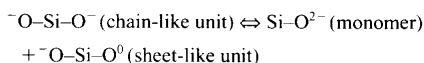
Comparative roles of Al³⁺ and Fe³⁺ ions for network construction in sodium silicate melts

M.MOHRI *et al.*

The Raman spectra of Na₂O–Al₂O₃–SiO₂ system with different Al₂O₃ contents (up to 25 mol%) and with Na₂O/SiO₂ ratio from 1 to 2 have been measured at 1 673 K.

In the disilicate systems, the Raman spectra do not change significantly with increasing of Al₂O₃ content except the development of the 500 cm⁻¹ band which is assigned to the three-dimensional network structural unit consisted of Si⁴⁺ and Al³⁺ ions. Also it is found that Al³⁺ ions possibly interact with monomers and form three-dimensional structures.

In the metasilicate systems, intensities of 950 and 850 cm⁻¹ bands gradually decrease while that of 1 100 cm⁻¹ band increases with the increase of Al₂O₃ content. According to the following equilibrium reaction in the metasilicate composition,



it is confirmed that Al³⁺ ions in the metasilicate systems do not interact with the polymerized silicate anions, such as chain-like or sheet-like structural units. On the other hand, it has a high tendency to interact with SiO₄⁴⁻ and construct three-dimensional network units involving Al³⁺ and Si⁴⁺ ions randomly. So it is obvious that the role of Al³⁺ ions for constructing the network structure is found to be quite different from that of Fe³⁺.

(*cf. ISIJ Int.*, **41** (2001), 410)

Mechanisms of carburization and melting of iron by CO gas

T.MURAKAMI *et al.*

Mechanisms of carburizing and melting iron in CO atmosphere with carbon activity of unity have been studied at a temperature range of 1 486–1 664 K, *i.e.* above the eutectic temperature of the Fe–C system. The behavior of melting iron was observed *in situ* by a confocal scanning laser microscope incorporated with an infrared image furnace. Carburization to γ -iron is controlled by the mixed rate-determining step, which consists of the carbon diffusion in γ -iron and chemical reaction at the gas–solid interface. The diffusion coefficient of carbon in γ -iron was determined from the carbon concentration profiles as follows,

$$D/m^2s^{-1} = 2.0 \times 10^{-6} \exp(-112.0 \times 10^3/RT) \quad (1\ 486 - 1\ 664\ \text{K})$$

where R is the gas constant, 8.314 JK⁻¹ mol⁻¹. The mechanism of iron melting by carburization is discussed according to the analogous treatment to the heterogeneous nucleation theory. An incubation time is necessary for melting iron, where the incubation time is the time required for the carbon concentration to reach the supersaturated concentration from the solidus concentration of carbon.

(*cf. ISIJ Int.*, **41** (2001), 416)

Steelmaking

Fluid slag skimming from steel ladles

K.WING *et al.*

A 1/7 scale model was constructed to physically simulate the skimming process of desulphurization slag from the transfer ladle used in the steelmaking industry. 1-decanol and water were used to represent the slag and the underlying molten steel, respectively. It was observed that the underlying liquid surface circulation created by three impinging gas jets in glancing contact with the bath surface would carry the slag towards the skimming mouth. The Reynolds number of the jets (I.D. 0.01 m) inclined 50° to the horizontal was 6 100. In the same amount of time, 70% of the slag originally charged to the tank was skimmed with the assistance of the jets in comparison to 20% when no jets were used. This approach to slag flow control was considered much more effective and less generally damaging than the use of submerged gas injection.

(*cf. ISIJ Int.*, **41** (2001), 422)

A mathematical simulator for the EAF steelmaking process using direct reduced iron

R.D.MORALES *et al.*

A mathematical simulator for the melting operation of direct reduced iron in electric arc furnaces (EAF) has been developed. The simulator takes into account the changes of physical properties of slag with time as well as the operating aspects of the process by using different input types of the raw materials into the furnace. Control of the bath oxidation is performed through the injection of carbon fines in the slag. Cost-optimized mass and energy

balances are employed as generators of initial and boundary conditions to start the solution of a set of ordinary differential equations whose solution allows to know the dynamic changes of temperature and metal and slag chemistry with time. Simulation results indicate that the final bath oxidation level is more dependent on the process routes than on the quality of the direct reduced iron (DRI) being melted. High carbon wettability by slags and basic slags are the most suitable conditions to promote iron oxide reduction in order to maintain a low bath oxidation. Process outputs influenced by complex EAF operations using different DRI metallizations, different sequences for feeding raw materials in the furnace, injection of carbon and oxygen and different types of inputs are well predicted by the present mathematical simulator.

(*cf. ISIJ Int.*, **41** (2001), 426)

Casting and Solidification

A modified cellular automaton model for the simulation of dendritic growth in solidification of alloys

M.FZHU *et al.*

A modified cellular automaton model (MCA) was developed in order to simulate the evolution of dendritic microstructures in solidification of alloys. Different from the classical cellular automata in which only the temperature field was calculated, this model also included the solute redistribution both in liquid and solid during solidification. The finite volume method, which was coupled with the cellular automaton model, was used to calculate the temperature and solute fields in the domain. The relationship between the growth velocity of a dendrite tip and the local undercooling was calculated according to the KGT (Kurz–Giovannola–Trivedi) model. The effects of constitutional undercooling and curvature undercooling on the equilibrium interface temperature were also considered in the present model. The MCA model was applied to predict the dendritic microstructures, such as the free dendritic growth from an undercooled melt and competitive dendritic growth in practical casting solidification. The simulated results were compared with those obtained experimentally.

(*cf. ISIJ Int.*, **41** (2001), 436)

Instrumentation Control and System Engineering

Optimization search algorithm of allocation planning for strip coils in hold for shipment by using operational know-how

T.UMEDA *et al.*

In the allocation planning of steel products in the hold of a ship, because the restriction which should be considered is complex and the problem scale is very large, planning systematization was difficult in the past. In this paper we study a scheduling algorithm of the allocation problem of steel products such as strip coils and sheets in the hold of a ship. Since steel products are usually stowed hierarchically in a hold, this planning becomes a three-dimensional allocation problem. First, we express the

stowing-position of the products as three-dimensional integer coordinates, and model them as a combinatorial optimization problem. Next, the weight balance of the ship, loading ratio, and work efficiency of stowing are evaluated quantitatively, and they are optimized by applying the SA (Simulated Annealing) method. To obtain a preferable solution in practical time, we take the stowing know-how which the operators have in the evaluation function, and can make the search process efficient. In addition, to confirm the effectiveness of the proposed algorithm, several case studies have been carried out with actual data. Through the case studies, it has been found that the evaluation function involving the operation know-how term could reduce more unloaded coils assuring qualities of other evaluation items than the best solution obtained by the evaluation function without know-how term.

(cf. *ISIJ Int.*, **41** (2001), 446)

Forming Processing and Thermomechanical Treatment

Numerical simulation of successive collision of two liquid droplets with a solid wall

H. FUJIMOTO et al.

Spray jet impingement is widely used to cool hot solids in iron- and steel-making processes. Numerous droplets impinge onto a solid at random and interact with each other. The present study treats the deformation behavior of two liquid drops one by one impinging coaxially onto a solid. The system of Navier–Stokes equations for incompressible fluid flow in the axial coordinate system is solved by means of a finite difference method. The effect of surface tension, gravity, and wettability between the liquid and the solid is taken into account. First, the deformation behavior of a single drop onto a solid is examined and compared to the experimental data for model validation. Then, the collision of two drops in tandem with the solid is simulated. The effect of the distance between two drops on the deformation behavior is studied. The physics of interaction phenomena of droplets is investigated theoretically.

(cf. *ISIJ Int.*, **41** (2001), 454)

Welding and Joining

Nitride precipitation in weld HAZs of a duplex stainless steel

J. LIAO

In order to obtain more information on the precipitation of nitrides, especially cubic type nitride CrN in weld heat affected zones of duplex stainless steels, the microstructures of thermally simulated weld heat affected zones (HAZs) of a commercial duplex stainless steel were characterized. The precipitates in the simulated weld HAZs were carefully examined with a transmission electron microscope. Not only Cr₂N but also CrN was found in the weld HAZs. The CrN appeared as film-like or tiny platelet-like, and precipitated at the regions adjacent to rod-like Cr₂N precipitates of high density. The orientation relation between CrN and δ ferrite matrix was $[110]_{CrN}/[111]_{\delta}$ and $(001)_{CrN}/(1\bar{1}0)_{\delta}$.

Besides Cr, Fe, V and Mo were also detected in both the two types of nitrides. The CrN precipitation might be understood using previous thermodynamic analysis results of Fe–Cr–Ni–Mo–N system and considering the difference in the diffusibilities of chromium and nitrogen atoms in δ ferrite during cooling.

(cf. *ISIJ Int.*, **41** (2001), 460)

Transformations and Microstructures

Transformation textures during diffusional $\alpha \rightarrow \gamma \rightarrow \alpha$ phase transformations in ferritic steels

G. BRÜCKNER et al.

The crystallographic transformation textures of a microalloyed low carbon steel were studied using X-ray and neutron diffraction techniques. Both with X-rays and with neutron radiation special equipment allowed to conduct *in situ* texture measurements at high temperatures, *i.e.* the determination of the texture evolution during rather than subsequent to annealing. The texture measurements were carried out in the ferritic regime at room temperature, after transformation into austenite at 950°C, and after back transformation into ferrite. Furthermore, the temporal evolution of texture was studied by measurement of textures in the $\alpha + \gamma$ two phase region with progressing transformation.

The $\alpha \rightarrow \gamma$ transformation degraded the texture sharpness, while during the $\gamma \rightarrow \alpha$ transformation the texture intensity decreased only slightly. Qualitatively the final ferrite texture after $\alpha \rightarrow \gamma \rightarrow \alpha$ transformation was inherited from the initial ferrite texture. Based on the experimental data transformation textures were calculated using the Kurdjumov–Sachs relation and compared with the experimental transformation textures. Differences between experimental and calculated transformation textures were obtained and attributed to variant selection. For the $\alpha \rightarrow \gamma$ transformation variant selection was associated with both dislocations and residual stresses interacting with strain caused by the volume change during transformation. The employed variant selection model depends on the grain orientation through the history of the initial grain. The variant selection during the $\gamma \rightarrow \alpha$ transformation is proposed to be caused by crystallographic constraints.

(cf. *ISIJ Int.*, **41** (2001), 468)

The temperature dependence of abnormal grain growth and grain boundary faceting in 316L stainless steel

J. S. CHOI et al.

When commercial 316L stainless steel specimens are heat-treated in a single phase state at 1100°C, abnormal grain growth (AGG) occurs and some grain boundaries are observed to be faceted with hill-and-valley structures in transmission electron microscopy. Some segments of these faceted grain boundaries are expected to be singular. When heat-treated at 1300°C normal grain growth occurs with all grain boundaries smoothly curved. These grain boundaries are expected to be atomically rough. At 1200°C AGG still occurs but there is no excessively large grain as in the specimen heat-treated at

1100°C. This correlation between the grain boundary structure and grain growth is consistent with those observed previously in pure metals, oxides, and a single phase model alloy. The occurrence of AGG with faceted grain boundaries is attributed to grain boundary movement with boundary steps either produced by two-dimensional nucleation or existing at the junctions with dislocations. As the grain boundaries become rough at 1300°C normal growth occurs because the grain boundaries migrate continuously with their rate expected to increase linearly with the driving force arising from the size difference. If a specimen heat-treated at 1100°C is further heat-treated at 1300°C, the AGG mode appears to switch to normal growth.

(cf. *ISIJ Int.*, **41** (2001), 478)

AlN precipitation in dual-phase 3% Si electrical steels

J.-H. OH et al.

The existing approaches to the detection of precipitation are largely based on room temperature measurements on quenched samples. However, the direct measurement of precipitation kinetics at high temperatures is also possible through analysis of the mechanical properties of the specimens. In this work, a creep method was developed and applied to the detection of aluminum nitride precipitation in a dual phase 3% silicon steel containing 0.038% C. Prior to loading, the specimens were solution treated for 20 min and then cooled to the test temperature. A constant stress was applied to each sample by means of a computerized MTS machine and the strain was recorded continuously during testing. Microstructural examination revealed that the austenite fraction and morphology and the microstructure of the ferrite matrix are quite different depending on whether samples are directly heated or heated and then cooled to the test temperature. The resulting creep rate is sensitive both to the occurrence of precipitation as well as to phase transformation; when the microstructure remains fixed, the slope of the true strain–log(time) curve decreases immediately after the initiation of precipitation. The precipitation-time-temperature diagrams determined in this way are of classical C shape.

(cf. *ISIJ Int.*, **41** (2001), 484)

Kinetics of phase transformations in steels: a new method for analysing dilatometric results

J. Z. ZHAO et al.

A dilatation curve records the detail of the phase transformation kinetics. The dilatometric technique may be applicable to the investigation of the phase transformation kinetics if the information contained in the dilatation curve can be extracted effectively. A detailed analysis has been made of the length change of a hypoeutectoid steel during a continuous cooling. A model has been developed in which the transient dilatation is calculated based on the fraction of the phases present. The model takes into account the redistribution of carbon and is applicable to the determination of the phase transformation kinetics from the dilatation data during a cooling of a hypo-eutectoid steel. The model was validated by

comparing the model results with the experimental results of an interstitial free steel. Experiments have been done with a bainitic steel. The model has been applied to the determination of the phase transformation kinetics from the dilatation curves of this steel. Excellent agreements between the model and experiments have been obtained.

(cf. *ISIJ Int.*, **41** (2001), 492)

Mechanical Properties

Effects of sulfur content and sulfide-forming elements addition on impact properties of ferrite-pearlitic microalloyed steels

N. TSUNEKAGE et al.

Longitudinal Charpy impact value of ferrite-pearlitic microalloyed steel was improved by large addition of S (0.05–0.1mass%), however, transverse Charpy impact value was rather deteriorated. This study focused on the sulfide shape, which have large effects on impact properties. The elements of Ca, Mg, Ti, and Zr were added to ferrite-pearlitic microalloyed steels with 0.1 mass% S for sulfide shape control, and their impact properties were compared. The addition of Ca or Mg to the steels improved the transverse Charpy impact value without changing the longitudinal Charpy impact value, while the addition of Ti or Zr to the steels resulted in deteriorating significantly both longitudinal and transverse Charpy impact values. The crack initiation energy of the Ca or Mg bearing steels improves by enlarge-

ment of the minute dimple area ratio in the ductile fracture surface because the elongation of sulfides in the hot forging process are controlled by the addition of Ca or Mg. On the other hand, the reason why the Charpy impact value of Ti or Zr bearing steels are deteriorated is that (Ti, V)C or plate type sulfides promote cleavage fracture and then raise their ductile-to-brittle transition temperature.

(cf. *ISIJ Int.*, **41** (2001), 498)

Social and Environmental Engineering

Immobilization mechanism of fluorine in aqueous solution with calcium aluminates

H. HE et al.

Immobilization of fluorine in aqueous solution with $3\text{CaO}\cdot\text{Al}_2\text{O}_3$ (C_3A) and $12\text{CaO}\cdot 7\text{Al}_2\text{O}_3$ (C_{12}A_7) has been investigated under the shaking and static conditions. The hydration products are identified by XRD and the microscopic observation has been made for the hydrated particles using electron microprobe analysis. It is found that the degree of immobilization of fluorine increases in the order of $\text{CA}_2 < \text{CA} < \text{C}_{12}\text{A}_7 < \text{C}_3\text{A}$ and the immobilization of fluorine occurs through the formation of $\text{Ca}_3\text{Al}_2(\text{OH})_{12-x}\text{F}_x$ and $\text{C}_3\text{A}\cdot\text{Ca}(\text{OH})_{2-x}\text{F}_x\cdot 18\text{H}_2\text{O}$. The former which contains a larger amount of F ($x=0-1.2$) is the major hydration product for hydrated C_3A , and the latter which contains a smaller amount of F ($x=0-0.12$) is the dominant phase for hydrated C_{12}A_7 . The conversion of the hexagonal

hydrates of $\text{C}_2\text{A}\cdot 8\text{H}_2\text{O}$ and $\text{C}_3\text{A}\cdot\text{Ca}(\text{OH})_2\cdot 18\text{H}_2\text{O}$ to the cubic hydrate of $\text{Ca}_3\text{Al}_2(\text{OH})_{12}$ occurs rapidly in the case of C_3A , while it occurs slowly in the case of C_{12}A_7 . During this conversion the F^- ion is incorporated into (OH^-) site in the $\text{Ca}_3\text{Al}_2(\text{OH})_{12}$ phase.

(cf. *ISIJ Int.*, **41** (2001), 506)

Effect of calcium silicates on immobilization of fluorine in aqueous solution

H. HE et al.

Immobilization of fluorine in aqueous solution with $2\text{CaO}\cdot\text{SiO}_2$ (C_2S) and $3\text{CaO}\cdot\text{SiO}_2$ (C_3S), and the effect of C_2S and C_3S on the fluorine immobilization with $3\text{CaO}\cdot\text{Al}_2\text{O}_3$ (C_3A) and $12\text{CaO}\cdot 7\text{Al}_2\text{O}_3$ (C_{12}A_7) have been studied. The hydration products are identified by X-ray diffraction method and the fluorine-substituted compounds are confirmed by electron microprobe analysis. It is found that C_3S appears more effective to immobilization of fluorine than C_2S and (OH^-) site in calcium silicate hydrates is substituted with F^- ion. The behavior of fluorine immobilization by calcium aluminates changes with the addition of calcium silicates because calcium silicates affect the formation of $\text{Ca}_3\text{Al}_2(\text{OH})_{12-x}\text{F}_x$, which is the most effective calcium aluminate hydrate in view of the incorporation of F^- ion. The fluorine immobilization with C_{12}A_7 can be promoted in the presence of appropriate amount of C_2S or C_3S .

(cf. *ISIJ Int.*, **41** (2001), 513)